Assessment of Skin Lesions Produced by Focused, Tunable, Mid-Infrared Chalcogenide Laser Radiation

Michael Evers,[1,2*] Linh Ha,[1,2] Malte Casper,[1,2] David Welford,[3] Garuna Kositratna,[1] Reginald Birngruber,[2] and Dieter Manstein[1]

[1]*Cutaneous Biology Research Center, Department of Dermatology, Massachusetts General Hospital, Harvard Medical School, Boston, Massachusetts*

[2]*Institute for Biomedical Optics, University of Lübeck, Lübeck, 23562, Germany*

[3]*Endeavour Laser Technologies, Inc., Hathorne, Massachusetts 01937*

Background: Traditionally, fractional laser treatments are performed with focused laser sources operating at a fixed wavelength. Using a tunable laser in the mid-infrared wavelength range, wavelength-dependent absorption properties on the ablation process and thermal damage formation were assessed with the goal to obtain customizable tissue ablations to provide guidance in finding optimized laser exposure parameters for clinical applications.

Methods: Laser tissue experiments were carried out on full thickness *ex vivo* human abdominal skin using a mid-infrared tunable chromium-doped zinc selenide/sulfide chalcogenide laser. The laser has two independent channels: a continuous wave (CW) output channel which covers a spectrum ranging from 2.4 μm to 3.0 μm with up to 9.2 W output power, and a pulsed output channel which ranges from 2.35 μm to 2.95 μm. The maximum pulse energy of the pulsed channel goes up to 2.8 mJ at 100 Hz to 1,000 Hz repetition rate with wavelength-dependent pulse durations of 4–7 ns.

Results: Total ablation depth, ablation efficiency, and coagulation zone thickness were highly correlated to wavelength, pulse width, and pulse energy. Using the same total radiant exposure at 2.85 μm wavelength resulted in 10-times smaller coagulation zones and 5-times deeper ablation craters for one hundred 6 ns pulses compared to one 100 ms pulse. For a fixed pulse duration of 6 ns and a total radiant exposure of 2.25 kJ/cm^2 the ablation depth increased with longer wavelengths.

Conclusion: The tunable laser system provides a useful research tool to investigate specific laser parameters such as wavelength on lesion shape, ablation depth and thermal tissue damage. It also allows for customization of the characteristics of laser lesions and therefore facilitates the selection of suitable laser parameters for optimized fractional laser treatments. Lasers Surg. Med. © 2018 Wiley Periodicals, Inc.

Key words: fractional ablation; tunable laser; pulsed ablation; CW; mid-infrared; thermal damage; human skin

INTRODUCTION

Mid-infrared laser radiation enables precise and selective ablation of biological tissue. Numerous clinically used laser systems are available and almost every medical subspecialty employs laser procedures [1]. Clinical laser tissue ablation is indicated by removal of small amounts of material while causing thermal damage, usually called the coagulation zone. Coagulated tissue can vary in size, discoloration, and charring depending on the laser parameters. Most commonly used lasers in the mid-infrared wavelength range are the 2.01 μm Tm:YAG laser [2], the 2.79 μm Er:YSGG laser [3], and the 2.94 μm Er:YAG laser [4] which emit close to or directly at the water absorption peaks of 2.0 μm and 2.94 μm [5]. Water is the main absorber of biological tissue in the mid-infrared wavelength range (Fig. 1) and the before mentioned lasers show significant differences in lesion shape and coagulation zone. While most laser parameters such as energy, spot size, pulse structure etc. and their interaction with biological tissue have been investigated intensively, wavelength-dependent ablation processes were restricted to specific lasers with fixed wavelengths due to the lack of tunable laser sources with sufficient energy.

Today, ablative and non-ablative fractional laser treatments are widely used in dermatology, for both aesthetic and medical indications such as remodeling of soft tissue, treatment of wrinkles, dyspigmentation, scars, and changes related to extrinsic skin aging [6,7]. Recently, fractional laser treatments are used to overcome the barrier function of the skin for topically applied agents [8]. Coagulated tissue and microchannels created by fractional laser treatments are used to penetrate deeper structures, enhance the therapeutic effect and evenly distribute

Conflict of Interest Disclosures: All authors have completed and submitted the ICMJE Form for Disclosure of Potential Conflicts of Interest and none were reported.

*Correspondence to: Michael Evers, Cutaneous Biology Research Center, Department of Dermatology, Massachusetts General Hospital, Harvard Medical School, 149 13th Street 3.233A, Boston, MA 02129.
E-mail: mevers@mgh.harvard.edu

Accepted 20 April 2018
Published online in Wiley Online Library (wileyonlinelibrary.com).
DOI 10.1002/lsm.22935

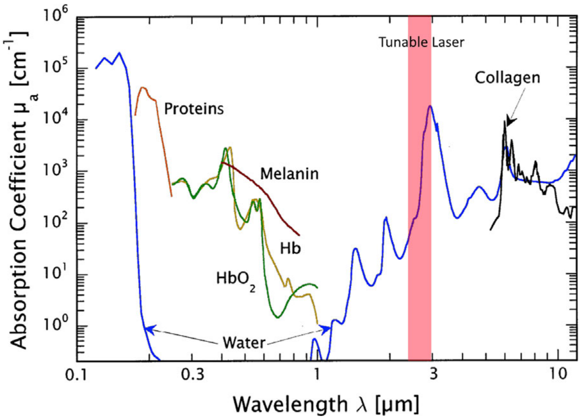

Fig. 1. Optical absorption coefficients μa of principal soft tissue chromophores are water, proteins, melanin, oxygenated hemoglobin (HbO_2), deoxygenated hemoglobin (Hb), and collagen, in the wavelength range from 100 nm to 10 μm [14].

topical agents in the dermal layer. This new emerging field of research is known as laser assisted drug delivery (LADD). Several recent publications showed a broad field of applications ranging from drug infiltration such as corticosteroid in scars [9], uptake of topical photosensitizers for photodynamic therapy [10], treatment with growth factors for hair loss [11], non-invasive patch-type transdermal vaccination [12] and transfer of bone marrow stem cells through the skin [13].

The interest in this field of research is growing rapidly and enhancement of clinical outcome can be achieved by optimization of several factors like delivery protocols, laser parameters and lesion characteristics. Haak et al. showed that the thickness of the coagulated zone of microchannels created by ablative fractional laser treatment have significant influence on the uptake of topically applied compounds [14]. Haedersdal et al. showed that ablative zones with thick coagulated tissue have a lower diffusivity which serve as a secondary diffusion barrier for drug delivery [15]. These coagulated zones can be used to create a drug reservoir in the microchannels to slow the release of drugs to the dermis.

Kositratna et al showed rapid formation of fibrin plugs in fractional lesions which could influence drug uptake and potentially be controlled by properties of the coagulation zone [16]. Lee et al presented that non-ablative fractional laser treatments assist cutaneous delivery of small- and macro- molecules through the skin with minimal bacterial infection risk [17]. Despite its common use for many indications, fractional laser treatments remain the risk of side-effects, such as hyperpigmentation, redness and burning. In order to reduce side-effects while attaining efficient therapeutic outcomes, it is essential to understand the light-skin interaction through evaluation of physical and physiological processes. These findings support and highlight the need to create customized lesions of different shapes, depths and coagulation zone for various applications. In this study, we used a continuously tunable chalcogenide laser system with a mid-IR wavelength range from 2350 nm to 3000 nm to investigate wavelength-dependent ablation processes. The continuous wavelength tunability of this laser source make it a suitable tool for research which is not restricted by a fixed wavelength. The effects of wavelength-dependent absorption properties on the ablation process and residual thermal damage formation in soft tissues was studied and compared to basic heuristic prediction models which enabled customizable lesion shape with controlled extent of thermal damage. Here, we demonstrated the capabilities of the mid-infrared tunable CW and ns-pulsed laser source and its interaction with soft tissue. By changing the system parameters such as energy per pulse, number of pulses and wavelength we were able to create highly customizable lesions in shape, depth and coagulation zone which eventually ensure maximized therapeutic outcome and minimal risk of side-effects for various applications. From a practical perspective, it is also important to note that tunable chalcogenide lasers have become commercially available and offer the possibility to conduct such experiments with relatively limited space requirements.

MATERIALS AND METHODS

Tunable Laser

The tunable chalcogenide laser (CW HTPTL-GS HETL-Integrated, IPG Photonics Corporation, Birmingham, AL) has two independent output channels: a CW channel and a ns-pulsed gain-switched channel. The ns-pulsed channel is based on a Cr^{2+}:ZnSe gain medium and is wavelength tunable from 2350 nm to 2950 nm. This channel has output energies of up to 2.8 mJ per pulse at 100–1,000 Hz and pulse durations of 4–7 ns. The maximum pulse energy and pulse duration vary depending on the repetition rate and wavelength.

The CW channel is based on a Cr^{2+}: ZnS crystal and wavelength tunable from 2400 and 3000 nm with output power levels of up to 9.2 W [18,19]. The CW and ns-pulsed laser beams have M^2 beam quality values of 3.5–5.6 and 1.5–1.8, respectively, depending on the wavelength. The laser beams of both modes of operation are focused by a lens system consisting of a meniscus and a plano-convex lens to an average $1/e^2$ spot size of 69 μm (3,739 μm^2) for the CW channel and 61 μm (2,922 μm^2) for the ns-pulsed channel as experimentally determined by the knife-edge method [20]. Attenuators were used to control the energy while keeping the beam profile consistent [21]. A micrometer translation stage was used to position the tissue specimen at the focal plane. An external shutter assembly (Uniblitz Vincent Associates, Rochester, NY) was added for both regimes of operation allowing the generation of down to 10 ms pulses/pulse trains. Dry nitrogen was used as a purge gas of the laser system to reduce absorptions in the mid-IR wavelength range since nitrogen has a homonuclear diatomic structure which does not absorb in the mid-infrared range [22]. Figure 2 shows the laser output energy per pulse of the pulsed laser operating at 400 Hz and the laser output power of the CW laser over the entire tunable spectrum at maximum pump power, after 1 hour of

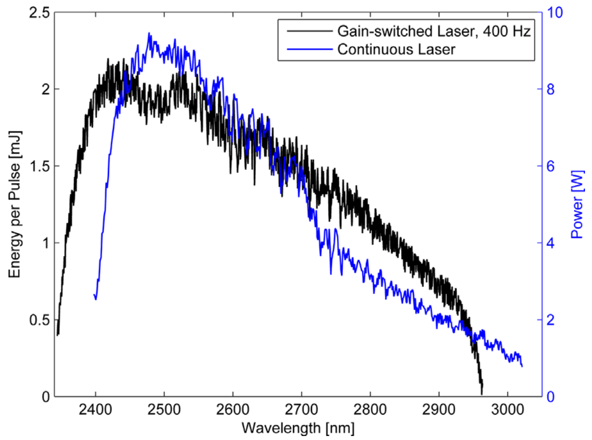

Fig. 2. The laser output energy per pulse of the gain switched ns-pulsed laser operating at 400 Hz over the entire tunable spectrum at maximum incident pump power, after one hour of purging. The peak energy per pulse in this figure is 2.2 mJ at 400 Hz. Longer purging results in higher peak energy and less water vapor absorption. The laser output power curve of the CW laser over the entire tunable spectrum at the maximum incident pump power of 40 W is also shown. The peak power for the CW regime of operation is 9.2 W.

purging. Both curves show strong fluctuations caused by water vapor which can be minimized by longer purging.

Preparation and Treatment of *Ex Vivo* Skin

Full thickness frozen *ex vivo* abdominal human skin samples were cut into small blocks and cleaned of fat, fascia, and hair. Thawed tissue samples were placed on a tissue assembly plate with the epidermal side up and covered by a $1 \times 20\,\text{mm}^2$ slit aperture and thermally equilibrated at room temperature.

Laser pulses were deployed through the slit aperture and the specimen were translated by a micrometer translation stage.

Exposed tissue samples were embedded in frozen OCT compound and 20 μm thick vertical sections were obtained by continuous cryo-sectioning. All sections were stained with nitroblue tetrazolium chloride (NBTC) and at least five individual lesions for each incident radiant exposure at each wavelength were analyzed and average values of lesion depth and thermally damaged zones were determined.

Thermal and Stress Confinement

The optical penetration depth δ, changes significantly across the wavelengths used in this work. The influence of heat conduction on energy deposition can be estimated by the thermal diffusion time τ_d [24]. Spatially confined effects can be achieved by using laser pulse durations that are shorter than the thermal diffusion time of the heated volume [25]. For laser ablation, the heated volume is typically a layer of the thickness of the optical penetration depth δ and the characteristic thermal diffusion time is given as:

$$\tau_d = \frac{1}{\mu_a^2 \kappa} = \frac{\delta^2}{\kappa} \tag{1}$$

where μ_a denotes the absorption coefficient, and $\kappa = 1.43 \times 10^{-3}\,\text{cm}^2\,\text{s}^{-1}$ is the thermal diffusivity of water [26]. For wavelengths with an optical penetration larger than the focused laser spot radius (about 33 μm) the following equation is used as defined by McKenzie et al. and Walsh et al. [24,27]

$$\tau_d = \frac{\delta^2}{4\kappa} \tag{2}$$

The laser wavelength, focused beam size, and pulse duration determine the confinement conditions in terms of stress generation and heat diffusion. In addition to rapid heating, short-pulse laser irradiation of tissue leads to the generation and propagation of thermo-elastic stresses. The stress confinement time τ_s is the time a stress wave needs to traverse through the directly heated volume of the tissue [21,28]:

$$\tau_s = \frac{\delta}{c_a} \tag{3}$$

where $c_a = 1{,}540$ m/s is the speed of sound in soft biological tissue [28]. When performing ablation under the conditions of stress confinement, the ablation process results in an increase of ablation efficiency and a reduction of thermal injury in the remaining tissue [29]. Table 1 shows wavelength dependent parameters like absorption coefficient and penetration depth, as well as the thermal confinement time and stress confinement time of skin. Looking at this table, one has to keep in mind that the human tissue used in this work has water contents from 30% (stratum corneum) to 70–80% (epidermis and dermis) and that the absorption coefficient also depends on temperature [30,31].

Metrics and Heuristic Models of Laser Ablation

The ablation threshold H_{th} of tissue determines the minimum required radiant exposure to achieve ablative material removal, which depends on the optical and mechanical tissue properties as well as on the lasers radiant exposure and pulse duration [32]. Different models are used to characterize and predict the outcome of laser ablation processes like the amount of removed material and thermal damage [33].

Typically, the theoretical ablation threshold which is needed for the vaporization of the entire target volume is much higher than the experimentally measured ablation threshold due to partially vaporized tissue and subsequent ejection of non-heated material. There are two fundamental ablation models, describing the extreme cases of absence of thermal diffusion (blow-off model) and thermal steady state conditions (steady-state model). These

TABLE 1. Thermal- and Stress-Confinement Time for Human Skin Using a Focused Beam With an Average Spot Size of 66 μm (Equations 1 and 2)

Skin (80% water)

Wavelength [nm]	Absorption coefficient [cm^{-1}]	Penetration depth [μm]	Thermal confinement [μs]	Stress confinement [ns]	Pulse duration [ns]
2400	40	250	546,000	160	4.7
2600	120	82	59,000	53	5.4
2750	2,160	5	50	3	5.4
2800	4,130	3	13	2	5.0
2850	6,530	2	5	1	5.9
2940	9,920	1	2	<1	7.5

The absorption coefficients are based on the product of absorption coefficient of water and the water content in the human skin (80%) as proposed by Chen et al. [23] The water absorption coefficients are based on experimental data from Hale and Querry [5]. The pulse duration for the pulsed regime of operation is shown for selected wavelengths at maximum pump power and 100 Hz repetition rate.

simplified laser tissue interaction simulations can be used as a guide for thermal profiles and ablation effects.

Blow-Off Model

The blow-off model assumes that the Lambert–Beer law accurately describes the spatial distribution of absorbed laser energy and that a finite threshold radiant exposure H_{th} is required to initiate ablation [24]. Due to using microbeams with small spot sizes and the fact that the vaporization is limited to a small fraction of the irradiated target volume, the latent heat of vaporization can be neglected and the ablation threshold can be reduced to a partial vaporization model [33]:

$$H_{\mathrm{th}} = \frac{1}{\mu_a}\varrho(c_v\Delta T) \tag{4}$$

where $\varrho = 1.05\,\mathrm{g/cm^3}$ is the density of skin, $c_v = 3.39\,\mathrm{J/gK}$ is the specific heat capacity of skin at $T_v = 373\,\mathrm{K}$, and $\Delta T = T_v - T_0$ is the absolute temperature rise [34]. Radiant exposures below the threshold only result in heating of the target. The model assumes that no material is removed during the laser pulse, which means that the material removal starts after the end of the laser irradiation. The model requires that the conditions for thermal confinement are satisfied. Wavelengths where the tissue absorption coefficient is large result in low threshold radiant exposure and small ablation depths δ_{abl}. Compared to that, lower absorption coefficients result in much larger threshold radiant exposures and deeper optical penetration. This shows a semi-logarithmic relationship between the ablation depth and the incident radiant exposure H_0 [29]:

$$\delta_{abl} = \frac{1}{\mu_a}\ln\left(\frac{H_0}{H_{th}}\right) \tag{5}$$

The depth of ablation, and thus, the volume of ablated material is dependent on the heat of ablation. The blow-off model provides no information about the physical mechanisms of the ablation process. It must be pointed out that this basic model does not consider parameters such as the influence of the tissue matrix or the temperature and pressure dependence of the absorption coefficient [35].

Steady-State Model

The steady-state model predicts that material removal occurs during the irradiation of the target linearly with time. It is used for microsecond and millisecond laser pulses. The ablation process and the removal of tissue mass begin as soon as the incident radiant exposure H_0 exceeds a fixed threshold H_{th}. Further, the model assumes that the removal of the material progresses at a constant rate during the entire laser pulse with the prediction of a linear relationship between ablation depth and radiant exposure [29]:

$$\delta_{\mathrm{abl}} = \frac{H_0 - H_{\mathrm{th}}}{\mu_a H_{\mathrm{th}}} \tag{6}$$

This approach describes a continuous ablation process in which the resulting material removal balances the irradiance delivered to the tissue, which is equivalent to the continuous-wave ablation theory. Compared to the blow-off model the development of the ablated crater depth is not logarithmic but linear with radiant exposure [36].

RESULTS

Short Pulsed (~5 ns) Ablation: Pulse Number Dependence

Multiple-pulse exposures were performed at 2400 nm and 2850 nm wavelength on *ex vivo* abdominal human skin with an average $1/e^2$ spot size of 61 μm (2,922 μm^2) to determine the relationship between number of pulses and ablation depth (Table 2). Tissue sections were exposed to 1, 4, 16, 64, 256, or 1024 pulses at 100 Hz repetition rate using maximum output resulting in 55 J/cm^2 radiant exposure per pulse (1.5 mJ per pulse) at 2400 nm or 22.5 J/cm^2 per pulse (0.6 mJ per pulse) at 2850 nm (Figs. 3 and 4). These

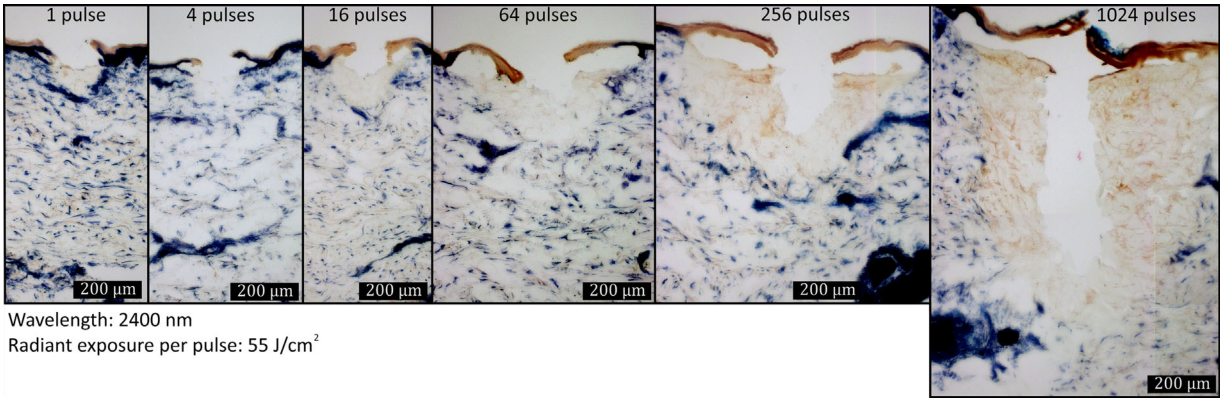

Fig. 3. Effect of different ~5 ns pulse numbers at 2400 nm wavelength with 55 J/cm^2 radiant exposure per pulse (1.5 mJ per pulse) at 100 Hz. Left to right: 1 pulse, 4 pulses, 16 pulses, 64 pulses, 256 pulses, 1,024 pulses.

are the highest achievable incident radiant exposures of the laser system at each wavelength which are well above the ablation threshold. The ablation crater size was measured from the tip of the crater to the top of the skin surface. The increase of pulse number resulted in deeper ablation craters for both wavelengths (Fig. 5A). The thickness of the thermal residual damage also increased significantly with the number of pulses, especially at 2400 nm wavelength. At both wavelengths, the ablation crater had a circular shape for lower pulse numbers and became conical as the number of pulses increased.

Pulsed (~5 ns) Ablation: Energy Dependence

Five different energies at 2400 and 2850 nm wavelength with an average 1/e^2 spot size of 61 µm (2922 µm^2) were applied to the tissue specimen to determine the relationship between radiant exposure and ablation depth. Tissue sections were exposed to 1 pulse of 33, 38, 44, 49, 55 J/cm^2 radiant exposures per pulse at 2400 nm and 10, 14, 15, 17, 19, 20 J/cm^2 radiant exposures per pulse at 2850 nm with 100 Hz repetition rate. The ablation craters became deeper for increasing radiant exposure per pulse for both wavelengths. The ablation threshold was determined by extrapolation of the data for material removal versus radiant exposure and resulted in 25.8 J/cm^2 at 2400 nm and 2.8 J/cm^2 at 2850 nm (Fig. 5B).

Long Pulse (100 ms) Ablation: Irradiance Dependence

Five different irradiances for different irradiances for 2400 and 2850 nm wavelength were applied to the tissue specimen for pulse durations of 100 ms with an average 1/e^2 spot size of 69 µm (3739 µm^2) (Table 3). Laser exposed tissue showed yellow discoloration for dermal tissue and

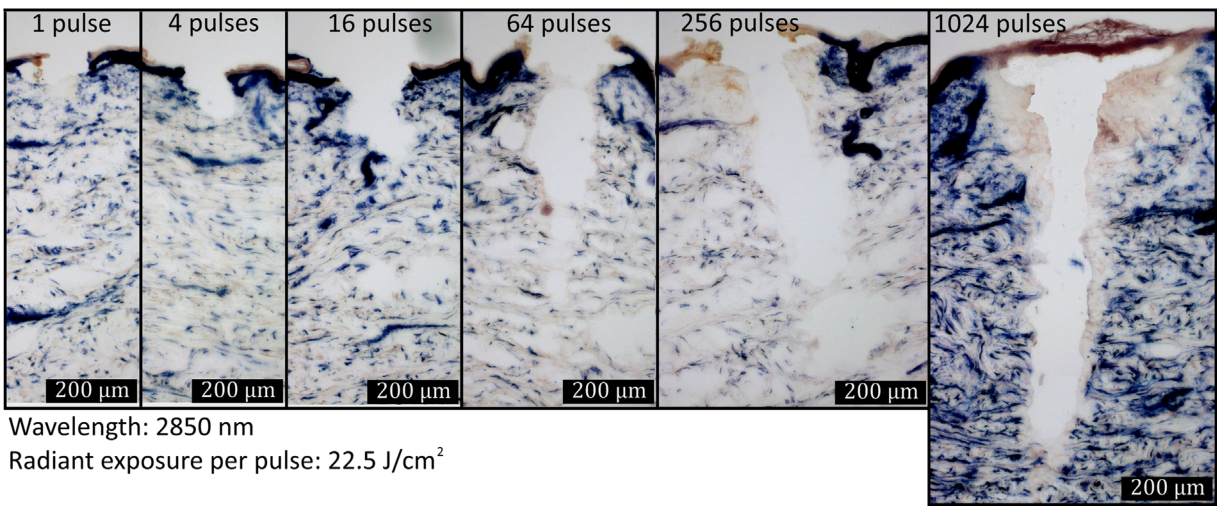

Fig. 4. Effect of different ~5 ns pulse numbers at 2850 nm wavelength with 22.5 J/cm^2 radiant exposure per pulse (0.6 mJ per pulse) at 100 Hz. Left to right: 1 pulse, 4 pulses, 16 pulses, 64 pulses, 256 pulses, 1024 pulses.

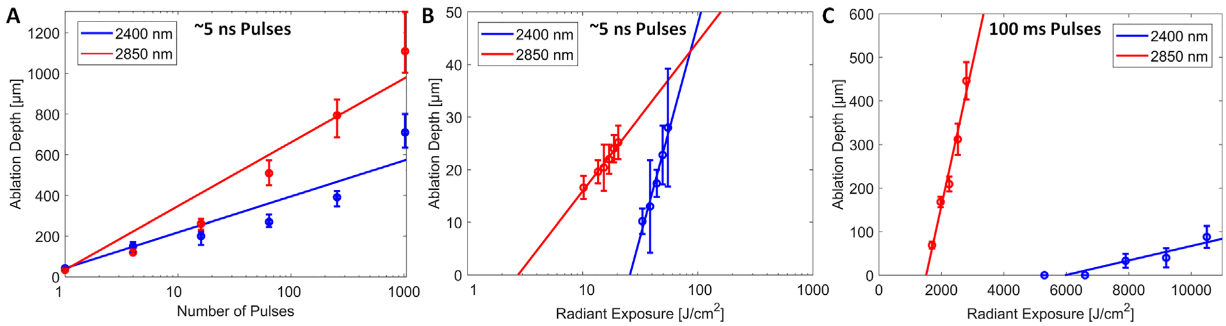

Fig. 5. Ablation depth measurements. **A**) Ablation depth of the ns-pulsed laser at 2400 nm wavelength with 55.0 J/cm^2 radiant exposure per pulse and at 2850 nm with 22.5 J/cm^2 at 100 Hz for increasing pulse numbers. **B**) Ablation depth at 2400 nm (33, 38, 44,49, 55 J/cm^2) and 2850 nm (10, 14, 15, 17, 19, 20 J/cm^2) wavelength of ~5 ns pulses at different radiant exposures. A logarithmic curve fit of the ablation depth, as determined by the blow-off model (Equation 5), was performed, based on a least square algorithm. (**C**) Ablation depth at 2400 nm and 2850 nm wavelength of 100 ms pulses at different radiant exposures. A linear curve fit of the ablation depth, as determined by the steady-state model (Equation 6), was performed, based on a least square algorithm.

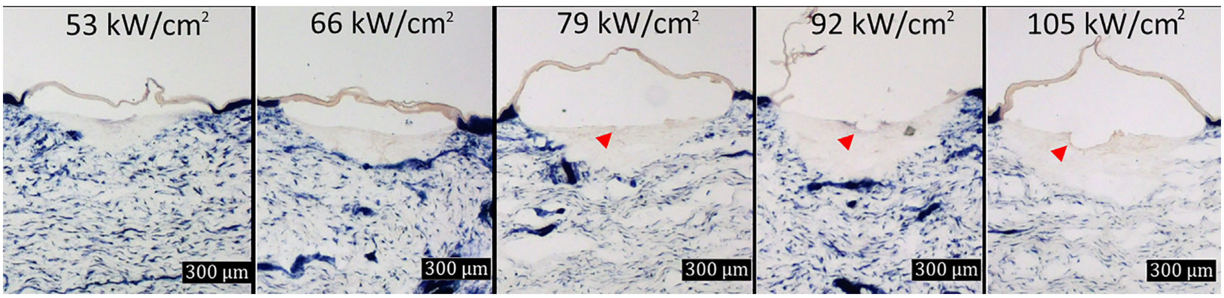

Fig. 6. Effect of different power levels per pulse with a pulse duration of 100 ms at 2400 nm wavelength of the CW laser. The irradiance was 53, 66, 79, 92, and 105 kW/cm^2 (200, 250, 300, 350, and 400 mJ per pulse, respectively).

dark yellow/brownish discoloration for epidermal tissue and stratum corneum on the NBTC stained vertical tissue sections (Figs. 6 and 7). The heat affected damage zones of coagulated collagen and epidermis were larger for 2400 nm wavelength compared to 2850 nm. The size of coagulated zones varied depending on irradiance, where lower power caused less thermal damage and higher power resulted in larger thermally damaged areas. The employment of higher power also led to deeper ablation. For the chosen irradiance, at 2850 nm wavelength the stratum corneum and epidermis were always ablated, whereas at 2400 nm wavelength they were fully or partially intact. During the ablation, especially for high power levels at long wavelengths, a tissue tightening effect was observed which can

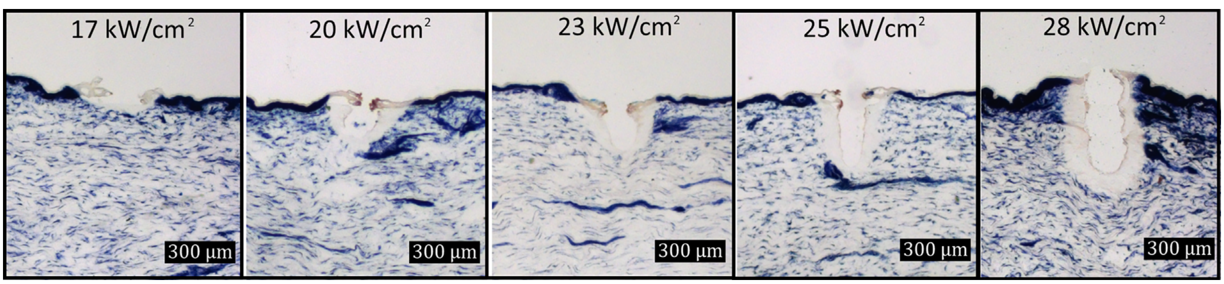

Fig. 7. Effect of different power levels per pulse with a pulse duration of 100 ms at 2850 nm wavelength of the CW laser. The irradiance was 17, 19.75, 22.5, 25.25, and 28 kW/cm^2 (60, 70, 80, 90, and 100 mJ per pulse, respectively).

be seen in the histology sections by deformation of the collagen bundle orientation (Fig. 7). The ablation threshold was determined by extrapolation of the data for material removal *vs.* radiant exposure and resulted in 6.0 kJ/cm^2 at 2400 nm and 1.5 kJ/cm^2 at 2850 nm (Fig. 5C).

Wavelength Dependence

Repetition rates of 100 Hz at 2400, 2600, 2750, 2800, and 2850 nm were used for the ns-pulsed laser and for the CW laser a power of 0.83 W at 2750, 2800, 2850, and 2940 nm with a pulse duration of 100 ms was used (Table 4). The total resulting radiant exposure for each setting on both lasers was approximately 2.25 kJ/cm^2. The selected power of 0.83 W determines the maximum power of the CW channel of the tunable laser system at 2940 nm. The NBTC stained vertical sections show notable changes in ablation depth and residual thermal damage zones; with increasing wavelength, the ablation depth increased while size of the thermal residual damage zones decreased (Figs. 8 and 9).

In addition to wavelength, the ablation process is also affected by pulse duration and peak power of the laser beam, and therefore thermal and stress confinement. Figure 10 shows the influence of beam characteristics on ablation depth and size of coagulation zone. Human skin was ablated with the ns-pulsed laser and the CW laser at different wavelengths with the same total radiant energy of 2.25 kJ/cm^2. The pulsed laser emitted 100 pulses at a frequency of 100 Hz and the CW laser used a single pulse of 100 ms. For according wavelengths (2750, 2800, and 2850 nm) the pulsed laser created significantly deeper ablation craters with less thermal injury compared to the CW laser.

DISSCUSION

Ablation Depth

In general, the ablation depth is dependent on wavelength, pulse duration, and incident radiant. Excitation at high absorbing wavelengths caused deeper ablation and narrower coagulation zones compared to excitation at lower absorbing wavelengths where a substantial portion of the energy went into heating and coagulation of the surrounding tissue. Excitation at low absorbing wavelengths decreased ablation efficiency while it increased thermal damage.

The relationship between pulse number and ablation depth of the pulsed laser was found to saturate with the number of pulses. At both wavelengths, for low pulse numbers, the ablation depth per pulse was significantly higher than for high pulse numbers where the tissue removal exhibited a saturating behavior (Table 5). Based on this saturation, a logarithmic approximation of ablation depth versus number of pulses was chosen (Fig. 5A). Other researchers have shown a similar saturation of ablation and coagulation depth for increasing pulse numbers in soft tissues such as human skin and human articular cartilage [37,38].

The saturation of the ablation versus depth curve has four additional reasons: (i) Skin is an inhomogeneous compound consisting of multiple layers; the epidermis dermis and subcutaneous tissue. The stratum corneum has the highest tensile strength of the skin, while the living epidermis has a lower tensile strength than the dermis which leads to more efficient ablation by the first pulses until the dermis with its high collagen content and therefore high mechanical strength is reached [29,30]. Collagen contraction which is evident by loop-like

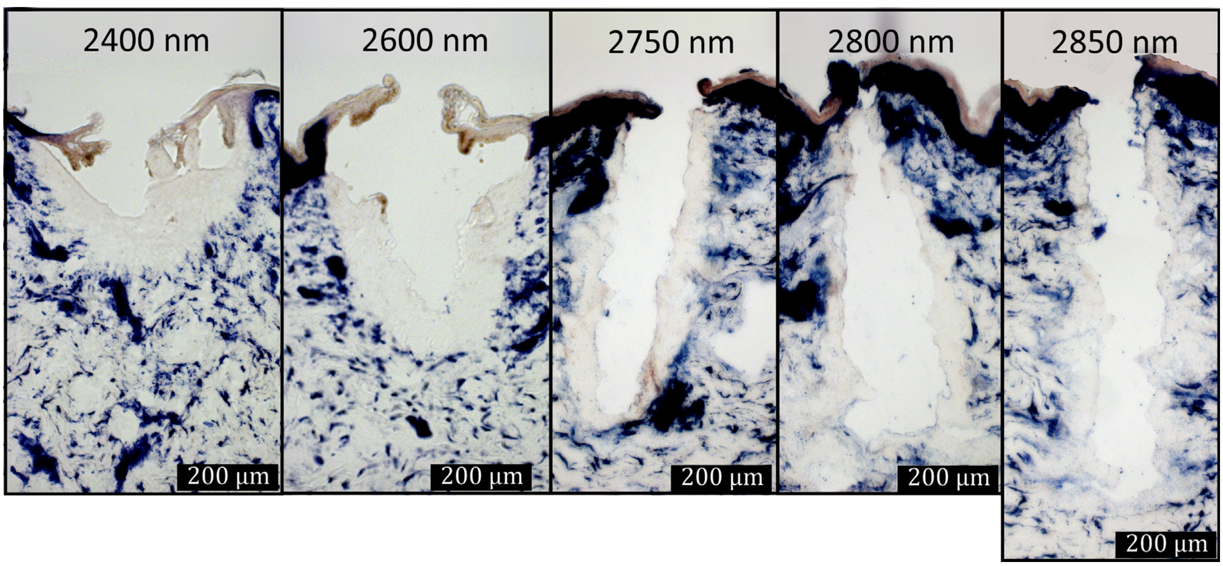

Fig. 8. Effect of different wavelengths at 2400, 2600, 2750, 2800, and 2850 nm (left to right) using 100 pulses with the ~5 ns-pulsed laser at 100 Hz resulting in a total incident radiant exposure of 2.25 kJ/cm^2 (0.6 mJ per pulse).

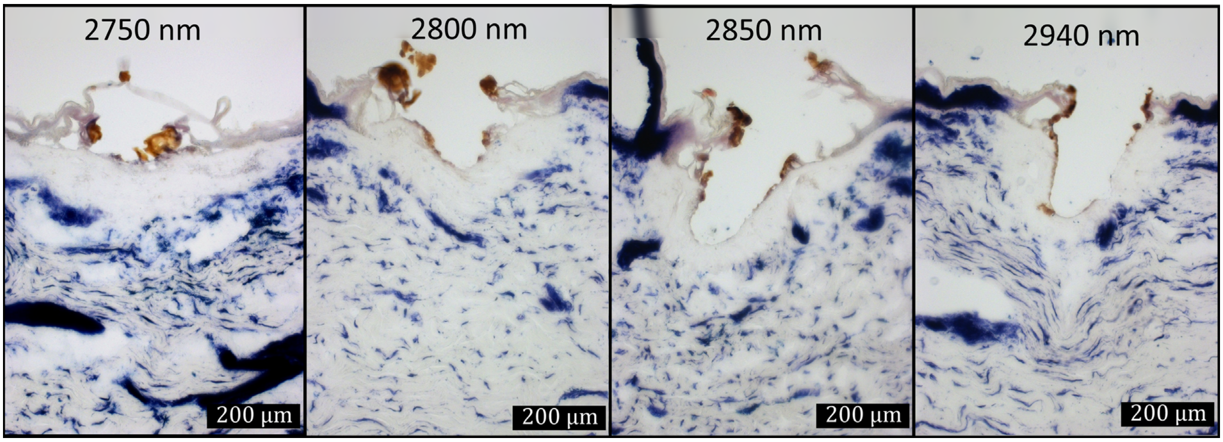

Fig. 9. Effect of different wavelengths at 2750, 2800, 2850, and 2940 nm (left to right) using 100 ms pulses with the CW laser at a constant power of 0.8 W resulting in a total incident radiant exposure of 2.25 kJ/cm^2 (80 mJ per pulse).

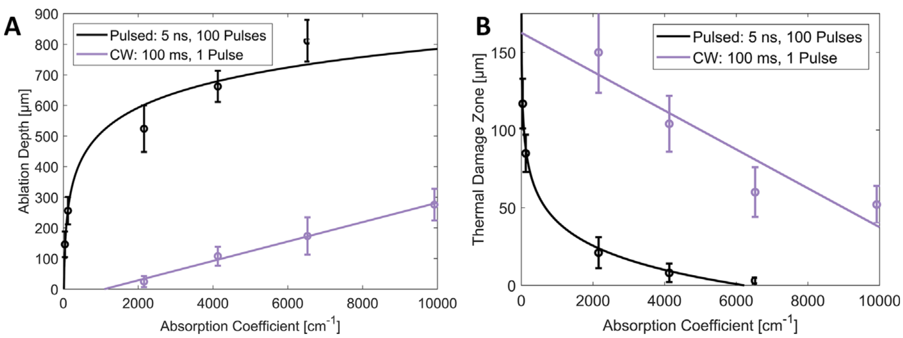

Fig. 10. (**A**) Ablation depth and (**B**) size of the thermal damage zone for different absorption coefficients. The measurements were done at the tip of the ablation crater for the pulsed and CW laser at different wavelengths in ex-vivo human abdominal skin. Hundred pulses of the pulsed laser at 22.5 J/cm^2 radiant energy and 100 Hz pulse repetition rate resulted in a total incident radiant energy of 2.25 kJ/cm^2. A single 100 ms pulse of the CW Laser at a constant power of 0.8 W resulted in an incident radiant exposure of 2.25 kJ/cm^2. A logarithmic fit was used for the data of the pulsed laser and a linear fit for the CW data.

distortion of the orientation of collagen bundles around ablation lesions might also affect the ablation efficiency; (ii) the laser focusing system used in this work focuses the beam at the tissue surface with a relatively short Rayleigh range of approximately 300 µm. This causes the energy density of the laser beam to decrease as the depth of the lesion increases; (iii) the visible formation of plasma at the tissue surface also led to a decrease of the optical

TABLE 2. Laser Parameter Settings for Pulse Number and Energy Dependency Experiments

	Pulse number dependence		Energy dependence	
Mode	Pulsed	Pulsed	Pulsed	Pulsed
Wavelength [nm]	2400	2850	2400	2850
Radiant exposure per pulse [J/cm^2]	55	22.5	33.0, 38.5, 44.1, 49.5, 55	10.2, 13.6, 15.3, 17.0, 18.7, 20.4
Number of pulses	1, 4, 16, 64, 256, 1024	1, 4, 16, 64, 256, 1024	5	5
Pulse width [ns]	4	4	4	7
Repetition rate [Hz]	100	100	100	100

TABLE 3. Laser Parameter Settings for Irradiance Dependency Experiments

	Irradiance dependence	
Mode	CW	CW
Wavelength [nm]	2400	2850
Irradiance [kW/ cm^2]	53, 66, 79, 92, 105	17, 19.75, 22.5, 25.25, 28
Number of pulses	1	1
Pulse width [ms]	100	100

transmission to the target. (iv) additional shielding effects such as absorption, scattering, and diffuse reflection of the laser beam by the ablation plume led to further attenuation and a reduction of the energy delivered to the target tissue. To minimize shielding, a vacuum hose was used to remove debris and ejected tissue material. We observed that the ablation plume, consisting of water droplets and ejected material, was successfully removed before the next laser pulse reached the tissue. While the vacuum hose efficiently removed ejected material from the tissue surface it was less efficient as the ablation front traversed deeper into the tissue and most of the ejected material stayed inside the laser drilled tissue channel.

Another shielding effect that occurred with the pulsed laser was the formation of plasma which were visually observed by a bright white flash at the tissue surface. The mechanism which led to laser induced breakdowns at short pulse durations is multi-photon ionization which was typically seen for longer wavelengths. Once plasma was ignited at high irradiation, most of the succeeding laser radiation was absorbed by the plasma, reducing the ablation efficiency. All abundant energy did not contribute to a further increase in ablation depth [39]. The relationship between radiant exposure and ablation depth of the pulsed laser was also found to saturate with increasing radiant exposure which can be explained by the blow-off model. At both wavelengths, once the ablation efficiency reaches a maximum it decreases monotonically at larger doses. Thus, for large radiant exposures much of the laser energy is used to heat superficial tissue layers far more than required for their removal [29]. Based on the blow-off model (Equation 5), a logarithmic approximation of ablation depth *vs.* radiant exposure was chosen (Fig. 5B). As predicted by the blow-off model, ablations at wavelengths with lower absorption coefficient have a higher ablation threshold but a steeper ablation depth *vs.* radiant exposure curve. Similar results were presented by Schomacker et al. using a tunable IR-laser to determine wavelength-dependent ablation thresholds of several tissue types with varying tensile strength. [40] Additionally, the laser ablation at 2400 nm is stress confined while at 2850 nm it is not, photoacoustic effects and thermos-elastic stress could explain higher ablation efficiency for high radiant exposures at 2400 nm wavelength compared to 2850 nm. While the logarithmic fit of Figure 5B represents the data well, the approximation is not perfect due to the simplicity of the blow-off model which neglects many aspects of the absorption process such as photoacoustic and photochemical effects. Nevertheless, the model can be used as a simple guide to describe ablation effects but cannot replace the *ex vivo* tissue analysis which would require far more sophisticated simulations. Hibst et al. also showed the logarithmic relation between ablation depth and radiant exposure due to shielding effects [41]. They unified the logarithmic blow-off model and the linear steady state model using a framework that accommodates the effects of plume absorption, or any other process reducing ablation efficiency, on the ablation process.

The ablation crater depth for the CW laser produced by 5 different power levels at 2400 nm and 2850 nm wavelength with 100 ms pulse duration was measured and found to increase monotonically with radiant exposure. A very satisfying linear least square curve fit was performed to approximate the relation between ablation depth and radiant exposure, as predicted by the steady state model (Equation 6) (Fig. 5C). As predicted by the steady state model, ablations at wavelengths with lower absorption coefficient have a higher ablation threshold and a lower ablation depth versus radiant exposure curve (Table 5).

Figure 10 shows that tissue ablation using the ~5 ns pulsed laser is 5–15 times more efficient than the CW laser in the wavelength range from 2700 nm to 2850 nm. This could be explained by the steady-state versus blow-off models and the greatly reduced residual thermal damage in the surrounding tissue caused by the ns-pulsed laser [25]. The peak pulse power of the pulsed laser is several fold higher than that of the continuous mode and the high laser light intensity causes the evaporation front to move into the tissue faster than the heat radiates outwards, minimizing residual thermal damage. Additionally, the ~5 ns pulsed laser is thermally and stress confined lowering the ablation threshold and increasing the ablation efficiency.

Thermal Damage

The epidermis and the dermis show varied thermal damage behavior. The differences can be explained by structural characteristics of the layers such as cell types, thickness, and water content. The stratum corneum and the living epidermis were often separated from the dermis after pulsed and CW laser irradiation. The separation and bulging could be explained by a loss of adhesive bond strength and thermally altered collagen caused by thermal laser effects [31].

Measurements at the bottom of the ablation crater defined the size of the coagulation zones. The ns-pulsed laser pulses were thermally confined for all used wavelengths; the absorbed laser energy was directly deposited and led to a temperature rise in the tissue which resulted in thermal damage with minimal heat diffusion to surrounding tissues. Figure 10 shows that tissue exposed to 100 pulses from the ns-pulsed laser operating at 2400 nm wavelength and 22.5 J/cm^2 radiant exposure per pulse, has a thermal damage depth of 117 μm. This is 53% less than the optical penetration depth of skin at 2400 nm wavelength (Table 1). This was explained by Walsh et al. who

TABLE 4. Laser Parameter Settings for Wavelength Dependency Experiments

Wavelength dependence		
Mode	Pulsed	CW
Wavelength [nm]	2400, 2600, 2750, 2800, 2850	2750, 2800, 2850, 2940
Total radiant exposure [kJ/cm^2]	2.25	2.25
Number of pulses	100	1
Pulse width	4–7 ns	100 ms
Repetition rate [Hz]	100	–

found that very thin zones of thermal damage were seen when radiant exposures were below or near the ablation threshold which was the case for the laser parameter settings at 2400 nm wavelength [42]. While for 2600, 2750, 2800, and 2850 nm wavelength the radiant exposure was well above the theoretical ablation threshold of skin, the coagulation zones exceeded the calculated optical penetration depth. Reasons for this are that human tissue used in this work has different water content of 30–80% depending on the layer, which increases the optical penetration depth and therefore the thermal damage depth. The increase of absorption coefficient of the ns-pulsed laser, while keeping the rest of the laser settings constant, led to coagulation zones which were at least 20 times smaller at 2850 nm wavelength compared to 2400 nm (Fig. 10).

The observation of very small thermally damaged zones, or even its absence, in soft biological tissue was made by Franjic and Jowett who used a 100 ps laser system at 2950 nm wavelength [43,44]. Similarly, we were able to show in this study that the pulsed laser with pulse durations of about 5 ns also produced ablation crater with very small thermally damaged zones in human skin. The reduction of the coagulation zone is a consequence of photoacoustic effects due to thermal and stress confinement. The thermo-elastic response of the tissue lowers the ablation threshold and this results in an increase of the ablation efficiency and a reduction of the thermal injury in the tissue that remains [35].

TABLE 5. Ablation Depth Per Pulse at 2400 nm Wavelength With 55.0 J/cm^2 Radiant Exposure Per Pulse and at 2850 nm Wavelength With 22.5 J/cm^2 Radiant Exposure Per Pulse, Both at 100 Hz for 1, 4, 16, 64, 256, and 1024 Pulses

Number of Pulses	Ablation Depth per Pulse[μm] at 2400 nm	Ablation Depth per Pulse [μm] at 2850 nm
1	42	34
4	38	30
16	13	16
64	4	8
256	2	3
1024	1	1

Increased coagulation zones could be observed at the tissue surface and at the ablation crater sides for high pulse numbers. Similar characteristics were observed by Walsh et al. and an explanation for this effect could be the development of hot gas [42]. The alterations observed at the edge of the ablation crater suggests that hot pressurized gases form during the ablation which are capable of thermally damaging and tearing the tissue. Furthermore, when material particularly deep within the tissue is vaporized, it cannot easily expand. It is, therefore, likely that the vaporization temperature of the tissue rises and thermal damage of the surrounding, non-ablated tissue increases.In contrast to thermal damage zones of the pulsed laser, damage zones of the CW laser were of almost uniform thickness at the ablation crater sides and at the bottom, implicating homogeneous heat conduction in all directions. Additionally, the 100 ms pulses of the CW laser did not fulfill the conditions of thermal confinement (Table 1). Again, the width of the thermal damage zones at 2750, 2800, 2850, and 2940 nm were significantly larger than the theoretical optical penetration depths at these wavelengths. We showed that the thermal damage could be directly controlled by pulse duration and radiant exposure. Even with low incident radiant exposures and 100 ms pulses at wavelengths with high absorption coefficients, thermal damage zones were up to 10 times larger than those obtained from the ns-pulsed laser.

CONCLUSION

This paper presents, for the first time, a tunable mid-infrared Cr^{2+}:ZnS/Se laser chalcogenide system that generates highly modifiable laser lesions in terms of shape, depth and size of the coagulation zone. This is possible due to the unique characteristics of the laser system such as a CW and ~5 ns pulsed mode of operation in the wavelength range of 2350 nm to 3000 nm with sufficient energy/power to ablate biological tissue. In order to perform systematic laser tissue ablation experiments on *ex vivo* abdominal human skin an experimental setup for the CW and ns-pulsed mode of operation were developed. We showed that the outcome of lesions was highly dependent on variation of radiant exposure, pulse duration and wavelength of the laser beam. For the CW mode of operation, coagulation zones are relatively thick for ablated and non-ablated lesions since the ablation is governed by heat diffusion due to relatively long pulse durations. We showed that the coagulation zones could be significantly decreased by change of laser excitation to highly absorbing wavelengths. Additionally, we showed that the CW laser ablation depth can be explained by the steady-state model with a linear relation of depth versus radiant exposure. In comparison to the CW mode, the pulsed mode used in this work with pulse durations of about 5 ns is capable to generate ablation craters with minimal thermal injury. The ablation depth of these craters can be described with the blow-off model and approximated with a logarithmic relation of radiant exposure *vs* depth.

The reduction of thermal damage zones for nanosecond pulses is a consequence of thermal and stress confinement effects. Compared to the ns-pulsed laser, in this wavelength range, the CW mode of operation required up to 200-fold more incident radiant exposure for the initiation of the ablation process. Further, we were able to show that increasing pulse numbers lead to deeper ablation craters as well as declining ablation efficiency.

For future work, the laser system could be used to systematically evaluate laser assisted drug delivery efficacy in relation to coagulation zone thickness and ablation crater depth. We showed that in contrast to traditional laser systems with a fixed wavelength the tunable laser source provides a unique opportunity to investigate effects of wavelength-dependent absorption properties on the ablation process and coagulation zone.

ACKNOWLEDGMENTS

We gratefully thank Martin Jaspan from Endeavour Laser Technologies Inc. and Dmitry Martyshkin from IPG Photonics Corporation for technical support and many technical discussions about the tunable laser system.

REFERENCES

1. Zeitler E, Wolbarsht ML. Laser characteristics that might be useful in biology. In: Laser applications in medicine and biology. Boston, MA: Springer; 1971. pp 1–18.
2. Spiegel J, Hansen C, Treede R-D. Clinical evaluation criteria for the assessment of impaired pain sensitivity by thulium-laser evoked potentials. Clin Neurophysiol 2000;111(4): 725–735.
3. Apel C, Meister J, Ioana RS, Franzen R, Hering P, Gutknecht N. The ablation threshold of Er:YAG and Er: YSGG laser radiation in dental enamel. Lasers Med Sci 2002;17(4): 246–252.
4. Lapidoth M, Yagima Odo ME, Odo LM. Novel use of Erbium: YAG (2,940-nm) laser for fractional ablative photothermolysis in the treatment of photodamaged facial skin: a pilot study. Dermatol Surg 2008;34(8):1048–1053.
5. Hale GM, Querry MR. Optical constants of water in the 200-nm to 200-m wavelength region. SPIE Milest Ser MS 1996;118:80–88.
6. Manstein D, Herron GS, Sink RK, Tanner H, Anderson RR. Fractional photothermolysis: a new concept for cutaneous remodeling using microscopic patterns of thermal injury. Lasers Surg Med 2004;34(5):426–438.
7. Issler-Fisher AC, Waibel JS, Donelan MB. Laser modulation of hypertrophic scars. Clin Plast Surg 2017;44(4):757–766.
8. Haedersdal M, Sakamoto FH, Farinelli WA, Doukas AG, Tam J, Anderson RR. Fractional CO_2 laser-assisted drug delivery. Lasers Surg Med 2010;42(2):113–122.
9. Waibel JS, Wulkan AJ, Shumaker PR. Treatment of hypertrophic scars using laser and laser assisted corticosteroid delivery. Lasers Surg Med 2013;45(3):135–140.
10. Bay C, Lerche CM, Ferrick B, Philipsen PA, Togsverd-Bo K, Haedersdal M. Comparison of physical pretreatment regimens to enhance protoporphyrin IX uptake in photodynamic therapy: a randomized clinical trial. JAMA Dermatol 2017;153(4):270.
11. Huang Y, Zhuo F, Li L. Enhancing hair growth in male androgenetic alopecia by a combination of fractional CO2 laser therapy and hair growth factors. Lasers Med Sci 2017; 1–8.
12. Scheiblhofer S, Strobl A, Hoepflinger V, et al. Skin vaccination via fractional infrared laser ablation—optimization of laser-parameters and adjuvantation. Vaccine 2017;35(14): 1802–1809.
13. Rodriguez-Menocal L, Salgado M, Davis S, et al. Percutaneous bone marrow transplantation using fractional ablative Erbium:YAG laser. PLoS ONE 2014;9(3):e93004.
14. Haak CS, Hannibal J, Paasch U, Anderson RR, Haedersdal M. Laser-induced thermal coagulation enhances skin uptake of topically applied compounds: LASER-INDUCED UPTAKE OF TOPICALLY APPLIED PEGs. Lasers Surg Med 2017; 49(6):582–591.
15. Haedersdal M, Sakamoto FH, Farinelli WA, Doukas AG, Tam J, Anderson RR. Pretreatment with ablative fractional laser changes kinetics and biodistribution of topical 5-aminolevulinic acid (ALA) and methyl aminolevulinate (MAL). Lasers Surg Med 2014;46(6):462–469.
16. Kositratna G, Evers M, Sajjadi A, Manstein D. Rapid fibrin plug formation within cutaneous ablative fractional CO2 laser lesions. Lasers Surg Med 2016;48(2):125–132.
17. Lee W-R, Shen SC, Aljuffali IA, Lin YK, Huang CW, Fang JY. Non-ablative fractional laser assists cutaneous delivery of small- and macro-molecules with minimal bacterial infection risk. Eur J Pharm Sci 2016;92:1–10.
18. Mirov SB, Fedorov VV, Moskalev IS, Martyshkin DV. Recent progress in transition-metal-doped II–VI mid-IR lasers. IEEE J Sel Top Quantum Electron 2007;13(3):810–822.
19. Moskalev IS, Fedorov VV, Mirov SB. 10-Watt, pure continuous-wave, polycrystalline Cr 2+: ZnS laser. Opt Express 2009;17(4):2048–2056.
20. de Araújo MA, Silva R, de Lima E, Pereira DP, de Oliveira PC. Measurement of Gaussian laser beam radius using the knife-edge technique: improvement on data analysis. Appl Opt 2009;48(2):393–396.
21. Ha ML. Fractional laser ablation of cutaneous tissue using a Tunable CW and gain-switched chromium-doped zinc chalcogenide IR laser. Master's thesis (University of Luebeck); 2012.
22. Kosters PGH. FT-IR spectroscopy of thin biological layers. PhD thesis (University of Twente); 2000.
23. Chen B, Thomsen SL, Thomas RJ, Welch AJ. Modeling thermal damage in skin from 2000-nm laser irradiation. J Biomed Opt 2006;11(6):064028.
24. Walsh JT, van Leeuwen TG, Jansen ED, Motamedi M, Welch AJ. Pulsed laser tissue interaction. In: Welch AJ, van Gemert MJC, editors. Optical-thermal response of laser-irradiated tissue. Netherlands, Dordrecht: Springer; 2010. pp 617–649.
25. Anderson RR, Parrish JA. Selective photothermolysis: precise microsurgery by selective absorption of pulsed radiation. Science 1983;220(4596):524–527.
26. Valvano JW. Tissue thermal properties and perfusion. In: Optical-thermal response of laser-irradiated Tissue. Dordrecht: Springer; 2010. pp 455–485.
27. McKenzie AL. Physics of thermal processes in laser-tissue interaction. Phys Med Biol 1990;35(9):1175.
28. Shin H-C, Prager R, Gomersall H, Kingsbury N, Treece G, Gee A. Estimation of average speed of sound using deconvolution of medical ultrasound data. Ultrasound Med Biol 2010;36(4):623–636.
29. Vogel A, Venugopalan V. Mechanisms of pulsed laser ablation of biological tissues. Chem Rev 2003;103(2):577–644.
30. Hendriks FM. Mechanical behaviour of human epidermal and dermal layers in vivo. Eindhoven: Technische Universiteit Eindhoven; 2005.
31. Walsh JT, Deutsch TF. Pulsed CO2 laser tissue ablation: measurement of the ablation rate. Lasers Surg Med 1988;8(3):264–275.
32. van Leeuwen TG, Jansen ED, Motamedi M, Welch AJ, Borst C. Excimer laser ablation of soft tissue: a study of the content of rapidly expanding and collapsing bubbles. IEEE J Quantum Electron 1994;30(5):1339–1345.
33. Jansen ED, van Leeuwen TG, Motamedi M, Borst C, Welch AJ. Partial vaporization model for pulsed mid-infrared laser ablation of water. J Appl Phys 1995;78(1):564–571.
34. Giering K, Lamprecht I, Minet O, et al. Specific heat capacities of human and animal tissues. Proc. SPIE 2624, Laser-Tissue Interaction and Tissue Optics, 1996. pp 188–197.
35. Apitz I. Analyse von Ablationsdynamik und akustischem Signal bei der gepulsten IR-Ablation biologischer Gewebe im

Hinblick auf eine Online-Ablationskontrolle. PhD thesis (University of Luebeck); 2006.
36. Olmes A, Franke HG, Baensch E, et al. Modeling of infrared soft-tissue photoablation process. Appl Phys B 1997;65(4-5):659–666.
37. Scheller EE. Neue Ansätze zur Knorpelgeweberestitution durch selektiven Wärmeeintrag mittels Laserstrahlung. Dissertation (Freie Universität Berlin, Freie Universität Berlin, Germany). Available at: http://www.diss.fu-berlin.de/diss/receive/FUDISS_thesis_000000017655 [Accessed September 14, 2017]; 2008.
38. Majaron B, Srinivas SM, Huang HL, Nelson JS. Deep coagulation of dermal collagen with repetitive Er:YAG laser irradiation. Lasers Surg Med 2000;26(2):215–222.
39. Niemz MH. Laser-tissue interactions. Berlin, Heidelberg: Springer Berlin Heidelberg; 2007. 10.1007/978-3-540-72192-5
40. Schomacker KT, Domankevitz Y, Flotte TJ, Deutsch TF. Co: MgF2 laser ablation of tissue: effect of wavelength on ablation threshold and thermal damage. Lasers Surg Med 1991;11(2): 141–151.
41. Hibst R. Technik, Wirkungsweise und medizinische Anwendungen von Holmium- und Erbium-Lasern (Ecomed); 1997.
42. Walsh JT, Flotte TJ, Deutsch TF. Er:YAG laser ablation of tissue: effect of pulse duration and tissue type on thermal damage. Lasers Surg Med 1989;9(4):314–326.
43. Franjic K, Miller RJD. Vibrationally excited ultrafast thermodynamic phase transitions at the water/air interface. Phys Chem Chem Phys 2010;12(20):5225.
44. Jowett N, Woellmer W, Reimer R, et al. Heat generation during ablation of porcine skin with Erbium:YAG laser vs a novel picosecond infrared laser. JAMA Otolaryngol Neck Surg 2013;139(8):828–833.